Oxidation of Metals, Vol. 48, Nos. 1/2, 1997

On the Oxidation of α-Fe and ε-Fe_2N_{1-z}: II. Residual Strains and Blisters in the Oxide Layer

Bart J. Kooi,† Marcel A. J. Somers,* Robin H. Jutte,‡ and Eric J. Mittemeijer*

Received January 25, 1996; revised November 18, 1996

The development of residual strains in the iron-oxide layers growing on α-Fe and ε-Fe_2N_{1-z} at 673 K in O_2 at 1 atm was investigated by X-ray diffraction at room temperature. After correction for thermal-strain development due to cooling after oxidation, it was found that tensile growth strains occur in magnetite and compressive growth strains occur in hematite. The growth strains in the oxides on α-Fe are (in absolute sense) 2–3 times as large as those in the oxides on ε-Fe_2N_{1-z}. Buckling of the oxide layer occurs in the case of an α-Fe substrate, which is attributed mainly to relaxation of the growth strains in magnetite and hematite. Thermal-strain development during cooling enhances the tendency for buckling. Buckling is not observed for oxide layers on ε-Fe_2N_{1-z}, which could be due to the smaller values of absolute strain in the oxide layer on ε-nitride. The absolute values of the growth strains in the oxide layer on ε-nitride being smaller is attributed to microstructural changes in the nitride layer during oxidation.

KEY WORDS: iron oxide; residual strain; growth strain; buckling.

INTRODUCTION

The resistance against atmospheric corrosion of a ferritic workpiece can be improved by application of a compound layer at the surface[1,2] composed of

* Laboratory of Materials Science, Delft University of Technology, Rotterdamseweg 137, NL-2628 AL Delft, The Netherlands.
† Present address: Department of Applied Physics, Materials Science Center, University of Groningen, Nijenborgh 4, NL-9747 AW Groningen, The Netherlands.
‡ Present address: Directorate-General of Public Works and Water Management, Road and Hydraulic Engineering Division, PO Box 5044, NL-2600 GA Delft, The Netherlands.

0030-770X/97/0800-0111$12.50/0

the iron-(carbo)nitrides ε-$Fe_2(N,C)_{1-z}$, and γ'-$Fe_4(N,C)_{1-x}$, as brought about by a nitriding (nitrocarburizing) treatment.[3] A further significant enhancement of the atmospheric corrosion resistance is realized by transformation of the surface adjacent part of the iron-nitride compound layer into iron oxide(s) by an oxidation treatment.[4,5] A thorough understanding of the origin of the improved corrosion resistance of oxidized ε-Fe_2N_{1-z} as compared to α-Fe is currently lacking. It has been suggested that this improvement is based on a different residual stress level in the oxide layer, such that the oxide layer adheres better to an ε-Fe_2N_{1-z} substrate than to an α-Fe substrate.[6,7]

The oxidation kinetics of α-Fe and ε-Fe_2N_{1-z} at 573 K and 673 K and the microstructural evolutions of nitride and oxide layers during oxidation was discussed in the preceeding paper.[8] This paper reports on the evolution of residual strains present in the oxide phases constituting the oxide layers on α-Fe and ε-Fe_2N_{1-z} at 673 K.

Relatively few published researches[9–14] dealt with the experimental determination of residual strains in iron-oxide layers generated by the oxidation of iron. In most cases the bent-strip method[9,10,12–14] was used to estimate the sign and the magnitude of the growth strain developing in the surface part of the oxidizing specimen. This method does not allow a distinction of strains in the several iron-oxide phases. So far, X-ray diffraction was not utilized to evaluate the lattice strains in the iron-oxide phases obtained on oxidizing pure α-Fe and ε-Fe_2N_{1-z}. The present paper reports the first results.

RESIDUAL STRAINS IN OXIDE LAYERS; GROWTH AND THERMAL MISFITS

Residual strains in oxide layers as determined at room temperature can result from a combination of a growth misfit introduced during oxidation and a thermal misfit between oxide layer and substrate imposed on cooling to room temperature after oxidation.

The occurrence and the value of the growth misfit in the growing oxide layer and/or between the growing oxide layer and the substrate is related to the growth mechanism of the oxide layer. Several mechanisms for the introduction of growth stresses in oxide layers have been proposed. Review papers covering this topic can be found, e.g., in Refs. 15–17.

For an oxide layer growing inwardly by anion-(oxygen) diffusion-controlled growth, new oxide is formed at the metal/oxide interface. Then, the ratio of the specific volume per metal atom/cation of the oxide layer and that of the substrate, i.e., the so-called Pilling-Bedworth ratio,[18] provides a value for the growth misfit. This origin of stress development in an oxide layer will not be considered further here, because this growth mechanism does not apply to the present iron-oxide layers.[8]

For an oxide layer growing outwardly by cation-(non-oxygen) diffusion-controlled growth, new oxide is formed at the outer surface. Then, the growth misfit may be accommodated by additional, outward-layer growth perpendicular to the surface. In such a case, which is likely to apply to the present case (cf. Ref. 8), growth strains can be absent. Nevertheless, growth strains have been generally observed to occur in oxide layers for which outward growth is rate controlled by cation transport to the surface. Several origins have been put forward to explain such strains. For example:[15–17]

- At a coherent interface between substrate and oxide layer a mismatch of the interatomic distances within the adjacent planes of oxide and substrate can lead to the introduction of a growth strain in the oxide layer (and the substrate). In general, changes of the atomic arrangement at the substrate side of the metal/oxide interface lead to a (change of the) constraint imposed on an adhering oxide layer and, consequently, growth strains develop or relax.
- Transition of a metal atom in the substrate to a cation in the oxide layer is associated with the creation of a vacancy at the substrate side of the metal/oxide interface. Such vacancies can be annihilated by inward movement of the interface[20] or by glide of dislocations.[19–21]
- A composition gradient can occur over the thickness of the oxide layer. Oxide formed at the surface is supposed to be stress free. On continued layer growth the cation concentration at a former surface location increases and, if no rearrangement of the oxygen anions is possible, an associated tendency to volume expansion leads to the introduction of compressive growth strains.
- Growth of a second oxide phase into an existing oxide phase, as for example the growth of magnetite into hematite on outward growth of the entire oxide layer, can be associated with the generation of residual strains in both oxide phases due to the difference in specific volume between the phases.
- In a polycrystalline oxide layer the development of oxide along existing oxide grain boundaries perpendicular to the surface, can result in the generation of compressive growth strains in the oxide layer. If microcracks or cavities exist within the oxide layer, the development of oxide along the surface of such heterogeneities can have a similar effect as oxide formation along grain boundaries.

It is noted that the occurrence of strain during growth may influence the growth mechanism, such that a reduction of the strain energy in the system takes place. For example, creep in the oxide layer (and in the substrate) and, more detrimental, buckling, and spallation of the oxide layer can occur.

The thermal misfit between oxide layer and substrate can be calculated from the difference in linear thermal expansion coefficient between layer and substrate and the temperature difference between oxidation temperature, T_2, and strain-measurement temperature, T_1. If the thermal misfit is accommodated fully and totally elastically by the oxide layer, the strain in the oxide layer parallel to the surface at temperature T_1 after cooling from temperature T_2, $\varepsilon_{\parallel}^{\text{th}}$, can be calculated from

$$\varepsilon_{\parallel}^{\text{th}} = \int_{T_2}^{T_1} (\alpha_{\text{sub}}(T) - \alpha_{\text{ox}}(T))\, dT \tag{1}$$

where α_{ox} and α_{sub} are the temperature-dependent linear expansion coefficients of oxide layer and substrate material, respectively.

EXPERIMENTAL PROCEDURES

Experimental details about the purity of the iron used, the oxidizing and nitriding treatments as well as the microscopical techniques have been given in the preceding paper.[8] All nitrided and oxidized iron samples subjected to X-Ray Diffraction (XRD) analysis for strain determination were of the Refined type (see Ref. 8).

XRD strain determination was performed with Siemens diffractometers of types F-ω and D-5000. The F-ω diffractometer was used with a line focus and was equipped with a curved graphite monochromator in the diffracted beam. The D-5000 instrument was used with a point focus and was equipped with a K_β-filter in the diffracted beam.

For the determination of the lattice strains in Fe_3O_4 the {533} CrK_α diffraction-line profile was measured with the F-ω diffractometer for values of $\sin^2\omega$ ranging from 0 to 0.5 employing positive ω tilt. (The angle ω plays the role of ψ in the so-called $\sin^2\psi$ analysis performed;[22,23] see Residual Strains in Oxide Layers section.) For the determination of the lattice strains in α-Fe_2O_3 the {104} CrK_α diffraction-line profile was measured with the D-5000 diffractometer for values of $\sin^2\psi$ ranging from 0 to 0.8 for both positive and negative ψ tilt. The diffraction-line profiles measured for the determination of lattice strains were corrected for (i) the dead time of the counting system (ii) a linear background by a least squares fit through the extremities of the profile and (iii) the angle dependent Lorentz-polarization[24] and absorption factors.[25] The peak maximum was obtained from the top of a parabola fitted by a least-squares procedure to the data in the peak region of the profile. Small errors in peak position due to defocussing of the goniometer were corrected for by calibration of the 2Θ and the ω or ψ scales with (strain-free) well-defined powder standards of Si and α-Fe_2O_3 powders on Si wafers, which were

prepared according to the method described in Ref. 26. The experimental error in the data presented here for the stress/strain perpendicular to the specimen surface normal was estimated to be $\Delta\sigma_{\parallel} = \pm 25$ MPa for the residual stress, corresponding to $\Delta\varepsilon_{\parallel} = \pm 0.008\%$ for the residual strain.

RESULTS AND INTERPRETATION

Residual Strains in Oxide Layers

Assuming a rotationally symmetric state of plane stress in the plane of the oxide layers, the value for the stress parallel to the surface, $\sigma_{\parallel}$, can be obtained from the slope of the straight line obtained by least-squares fitting through the experimental data in a plot of d_{ψ}^{HKL} vs. $\sin^2\psi$[22,23]

$$\varepsilon_{\psi}^{HKL} = \frac{d_{\psi}^{HKL} - d_{\varepsilon=0}^{HKL}}{d_{\varepsilon=0}^{HKL}} = 2S_1^{HKL}\sigma_{\parallel} + \tfrac{1}{2}S_2^{HKL}\sigma_{\parallel}\sin^2\psi \qquad (2)$$

where d_{ψ}^{HKL} is the HKL lattice spacing determined in a direction characterized by the angle ψ with respect to the surface normal, $d_{\varepsilon=0}^{HKL}$ is the strain-free lattice spacing, ε is the strain and S_1^{HKL} and $\frac{1}{2}S_2^{HKL}$ are the so-called X-ray elastic constants for the HKL reflection. Values for S_1^{HKL} and $\frac{1}{2}S_2^{HKL}$ of the oxide phases under consideration were calculated from the corresponding single crystal elastic constants,[21] using the Hill approximation, i.e., the mean of the values obtained according to the Voigt and Reuß approximations (see, e.g., Ref. 27), yielding for the analysis using the Fe_3O_4 {533} and the α-Fe_2O_3 {104} reflections

$$Fe_3O_4: \quad S_1^{533} = -1.09\ 10^{-6}\ MPa^{-1}; \qquad \tfrac{1}{2}S_2^{533} = 5.33\ 10^{-6}\ MPa^{-1}$$
$$\alpha\text{-}Fe_2O_3: S_1^{104} = -0.909\ 10^{-6}\ MPa^{-1}; \qquad \tfrac{1}{2}S_2^{104} = 5.58\ 10^{-6}\ MPa^{-1}$$

Residual stresses $\sigma_{\parallel}$ thus obtained are related to residual strains parallel to the plane of the oxide layer, $\varepsilon_{\parallel}$, by

$$\varepsilon_{\parallel} = \frac{1-\nu}{E}\sigma_{\parallel} \qquad (3)$$

with ν as Poisson's constant and E as Young's modulus of the polycrystalline oxides (for data, see Ref. 21).

Residual stresses and strains were determined for oxide layers obtained after oxidation times of 49, 100 and 225 min at 673 K both on α-Fe and on "dense" and "porous" ε-Fe_2N_{1-z} (cf. Ref. 8). The results obtained for the

Table Ia.[a]

	$\sigma_{\parallel}$ (MPa)					
Oxidation time	α-Fe		"Dense" ε-Fe_2N_{1-z}		"Porous" ε-Fe_2N_{1-z}	
(min)	Fe_3O_4	α-Fe_2O_3	Fe_3O_4	α-Fe_2O_3	Fe_3O_4	α-Fe_2O_3
49	[d]	−538	[d]	[d]	−70	−328
100	200	−465	12	−344	5	−368
225	101	−354	−42	−281	48	−195

Table Ib.[b]

	$\varepsilon_{\parallel}$ (%)					
Oxidation time	α-Fe		"Dense" ε-Fe_2N_{1-z}		"Porous" ε-Fe_2N_{1-z}	
(min)	Fe_3O_4	α-Fe_2O_3	Fe_3O_4	α-Fe_2O_3	Fe_3O_4	α-Fe_2O_3
49	[d]	−0.199	[d]	[d]	−0.024	−0.121
100	0.068	−0.172	0.004	−0.127	0.002	−0.136
225	0.034	−0.131	−0.014	−0.104	0.016	−0.072

Table Ic.[c]

	$\varepsilon_{\parallel}^{gr} = \varepsilon_{\parallel} - \varepsilon_{\parallel}^{th}$ (%)					
Oxidation time	α-Fe		"Dense" ε-Fe_2N_{1-z}		"Porous" ε-Fe_2N_{1-z}	
(min)	Fe_3O_4	α-Fe_2O_3	Fe_3O_4	α-Fe_2O_3	Fe_3O_4	α-Fe_2O_3
49	[d]	−0.105	[d]	[d]	0.012	−0.028
100	0.104	−0.079	0.040	−0.034	0.038	−0.043
225	0.070	−0.038	0.022	−0.011	0.052	+0.021

[a] Residual stress parallel to the layer/substrate interface, $\sigma_{\parallel}$, and [b] corresponding residual strain, $\varepsilon_{\parallel}$, in Fe_3O_4 and α-Fe_2O_3 phases grown upon oxidizing α-Fe (Refined) and dense and porous ε-Fe_2N_{1-z} substrates at 673 K in O_2 at 1 atm. [c] The residual strains after subtraction of the thermal strain imposed by the contraction of the ferrite substrate, using the data for the assemblies α-Fe_2O_3/α-Fe and Fe_3O_4/α-Fe given in Fig. 3b. After 49 min of oxidation both Fe_3O_4 and α-Fe_2O_3 were present in all oxide layers investigated (cf. Fig. 10 in Ref. 8). [d] However, in some cases, it was not possible to determine residual stresses/strains in both these phases (see Residual Strains in Oxide Layers section).

Fe_3O_4 and α-Fe_2O_3 phases are collected in Tables Ia and b. In all samples oxidized for 49 min oxidation both Fe_3O_4 and α-Fe_2O_3 were present (cf. Fig. 10 in Ref. 8). In some cases, however, it was not possible to determineresidual stresses/strains in these phases owing to very faint and broad diffraction peaks. This is indicated in Tables Ia–c. A typical graph of d_{ψ} vs. $\sin^2\psi$ is given in Fig. 1 for the α-Fe_2O_3 {104} line profile originating from α-Fe that is oxidized for 49 min at 673 K. Both positive and negative ψ tilts were

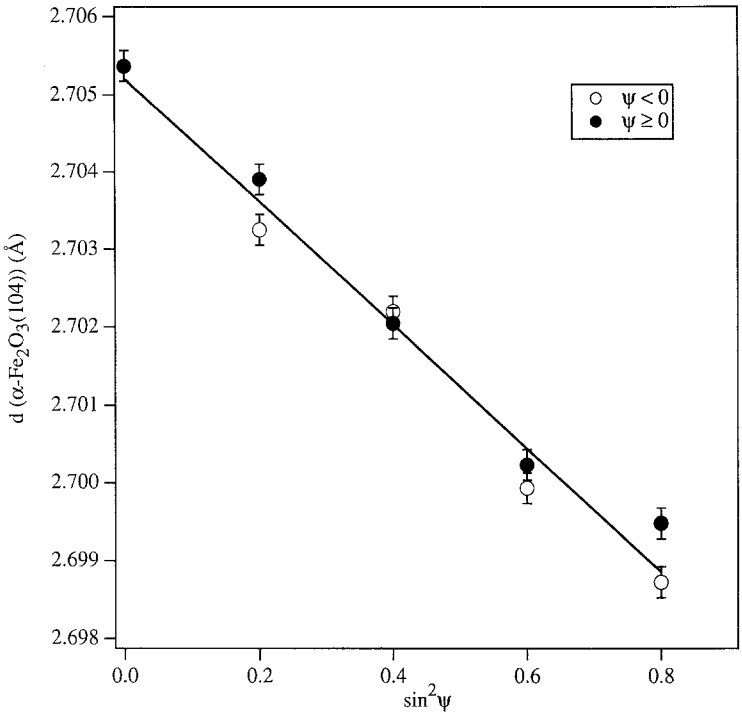

Fig. 1. The lattice spacing, d, as calculated from the {104} reflection of α-Fe_2O_3 as a function of $\sin^2\psi$ for an α-Fe (Refined) sample oxidized during 49 min at 673 K in O_2 at 1 atm. The negative slope of the straight line fitted by a least-squares procedure is indicative of a relatively large compressive residual stress parallel to the surface in the α-Fe_2O_3 layer. Both positive and negative ψ tilts were performed, resulting in two data points per $\sin^2\psi$ value for $\sin^2\psi \neq 0$. No ψ splitting is observed.

performed resulting in two data points for each $\sin^2\psi \neq 0$. The results for positive and negative ψ tilt do not differ significantly, i.e., no ψ splitting[35] occurs. Because all stresses (strains) are assumed to be within the plane of the oxide layer, the presence of oxide in pores of the porous ε-nitride layer will complicate the interpretation of the strain value determined, in particular for the relatively thin oxide layers obtained after short oxidation times. The occurrence of buckling of the oxide layer on α-Fe (see the following section and Ref. 8) also affects the interpretation of the strain value obtained, since a part of the diffracting oxide material will not be constrained by the substrate and can be relatively stress free. As a consequence the overall strain will be lower if buckling occurs and stress components in other directions than perpendicular to the specimen surface normal may occur.

The following conclusions can be drawn on the basis of the results of Table Ia/b for the strains in the oxide layers at room temperature:

(i) A large compressive stress/strain occurs in α-Fe_2O_3 on all substrates. Its absolute value decreases on continued oxidation;
(ii) The compressive stress/strain in α-Fe_2O_3 on α-Fe is larger than in α-Fe_2O_3 on ε-Fe_2N_{1-z} for the same oxidation time;
(iii) A significant tensile stress/strain occurs in Fe_3O_4 on α-Fe which decreases significantly on prolonged oxidation;
(iv) No significant stress/strain occurs in Fe_3O_4 on ε-Fe_2N_{1-z} (cf. Experimental Procedures section: $\Delta\sigma_{\parallel} = \pm 25$ MPa and $\Delta\varepsilon_{\parallel} = \pm 0.008\%$).

Blister Formation by Buckling of the Oxide Layer

Blister formation by buckling of the oxide layer occurred for α-Fe substrates upon oxidizing at both 573 K and 673 K. The onset of buckling of the oxide layer was found to depend on the oxidation temperature and appeared to coincide with the occurrence of magnetite in the oxide layer.[8]

A micrograph of the surface of α-Fe (J&M) oxidized at 573 K for 600 min shows fringes across the grains that manifest buckling of the oxide layer (Fig. 2): the fringes arise because of interference of the part of the applied monochromatic light that is reflected directly at the blister surface and the part that is transmitted through the blister (very thin oxide layer), after (multiple) reflection at the substrate surface and the substrate side of the blister. Taking the oxide layer as infinitely thin, it can be shown for the case of normal incidence of the applied monochromatic light that intensity minima (fringes) are observed if the height, h, of the blister above the substrate satisfies (cf. Ref. 36):

$$h = \frac{\lambda}{2n}\left(-m + \frac{\varphi}{2\pi}\right) \quad \text{for } m = 0, \pm 1, \pm 2, \ldots \tag{4}$$

where λ is the wavelength of the incident, monochromatic light; n is the refractive index of the vacuum ($n = 1$) in-between blister surface and substrate surface; φ is the phase shift occurring on reflection of light at the substrate surface ($\varphi = -0.438$ radians for ferrite and normal incidence of the light). In this case the first fringe occurs for $m = 1$. Thus, the fringes represent iso-height contours for the blister surface above the substrate; the height difference between successive fringes amounts to $\lambda/2$. On this basis, the height of the blister surface above the substrate is given in Fig. 2b as a function of the distance along the line indicated in Fig. 2a. The results of two sets of measurements performed with two different wavelengths of incident light agree very well (Fig. 2b).

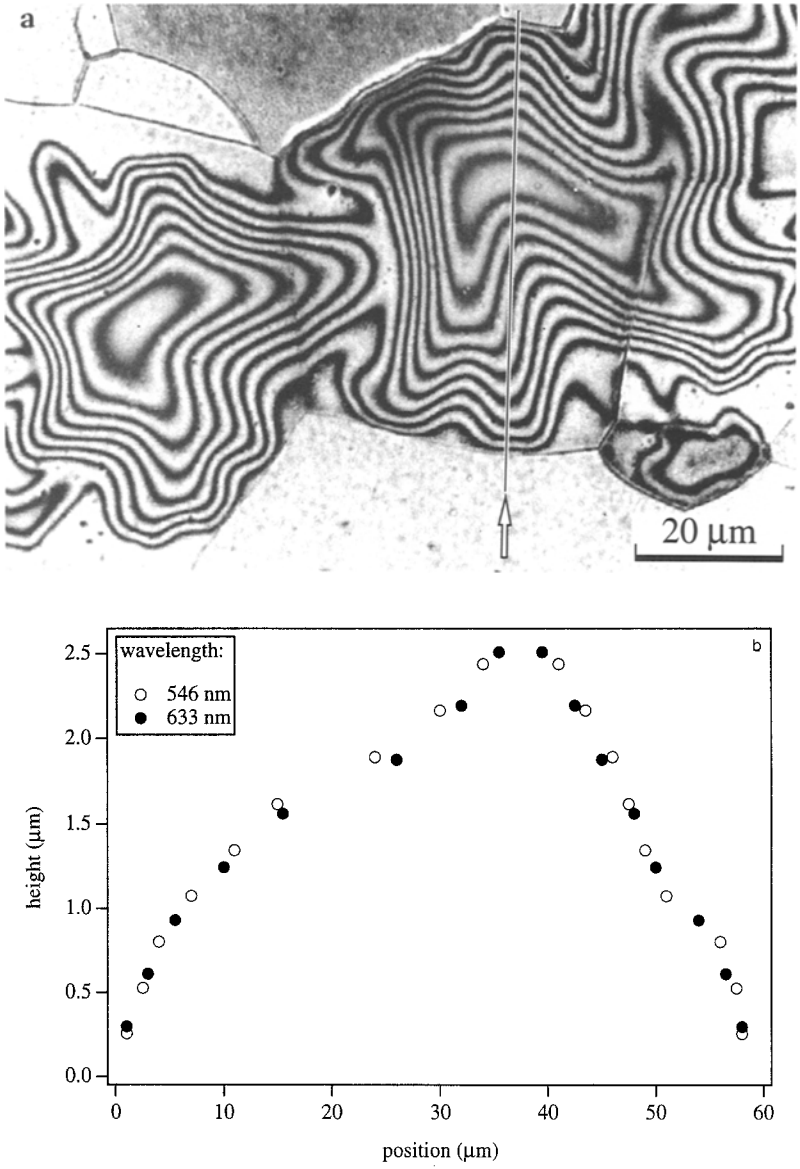

Fig. 2. (a) Micrograph (bright field, monochromatic light: 546 nm) of the surface of α-Fe (J&M) oxidized at 573 K for 600 min showing an interference (fringe) pattern. The fringes are interpreted as iso-height contours of the oxide blister. The height of the blister is shown as a function of the distance along the line indicated in the micrograph in (b) for 2 wavelengths of the normally incident monochromatic light.

DISCUSSION

Evaluation of Growth Strains in the Oxide Phases

The linear expansion coefficients of α-Fe,[28] Fe_3O_4 (average of curves from Ref. 29 as cited in Ref. 30), α-Fe_2O_3 (Ref. 31 as cited in Ref. 30) and ε-Fe_2N_{1-z}§ are given as a function of temperature in Fig. 3a. Assuming an infinitely thick substrate and fully elastic accommodation of the thermal misfit, the thermal strain in the oxide layer introduced on cooling from the oxidation temperature (T_2) to room temperature (T_1) can be calculated with Eq. (1) and the data in Fig. 3a. The results are given for several oxide/substrate combinations in Fig. 3b. The experimental strain values at room temperature (Table Ib) can then be corrected for the thermal strain imposed on cooling by the ferrite substrate, for both iron oxide on α-Fe and iron oxide on ε-Fe_2N_{1-z}. Thus resulting growth strains in the iron-oxide phases are given in Table Ic. It is concluded that, at the oxidation temperature, for all layer/substrate assemblies investigated a tensile growth strain occurs in magnetite; for all but one of the layer/substrate assemblies a compressive growth strain occurs in hematite.

Growth Strains in Oxide Layers on α-Fe

The growth strains in Table Ic cannot be ascribed unequivocally to just one of the mechanisms presented in the section Residual Strains in Oxide Layers; Growth and Thermal Misfits. In Ref. 8 it was shown that, for the present case, the oxide-layer growth is rate controlled by short-circuit diffusion of iron cations. Therefore, it may be suggested that the formation of oxide along the short circuits (e.g., grain boundaries) could be (partly) responsible for the compressive nature of the growth strains in hematite.

After some time Fe_3O_4 nucleates at the α-Fe/α-Fe_2O_3 interface and an Fe_3O_4/α- Fe_2O_3 interface develops within the original hematite layer.[8] On prolonged oxidation, this interface shifts in the direction of the surface. Consider a local transformation of α- Fe_2O_3 into Fe_3O_4 by supply of iron cations, while conserving the number of oxygen anions (because the cations are the diffusing species). Then, a compressive growth strain is expected in Fe_3O_4, because of the difference in specific volume (expressed per oxygen anion[11]) between magnetite and hematite. The observed tensile nature of the growth strain in Fe_3O_4 (Table Ic) is opposite to this expectation. It may be suggested that (i) rather than a mere transformation of the anion sublattice

§ The linear thermal expansion coefficient of ε-nitride was evaluated from the a and c lattice parameters of ε-nitride at 298 K and 609 K.[32] It was obtained for the linear expansion coefficient in the a direction 6.85 10^{-6} K^{-1} and for the linear expansion coefficient in the c direction 19.1 10^{-6} K^{-1}. Hence, the average linear expansion coefficient as determined from the volume expansion amounts to 10.9 10^{-6} K^{-1}.

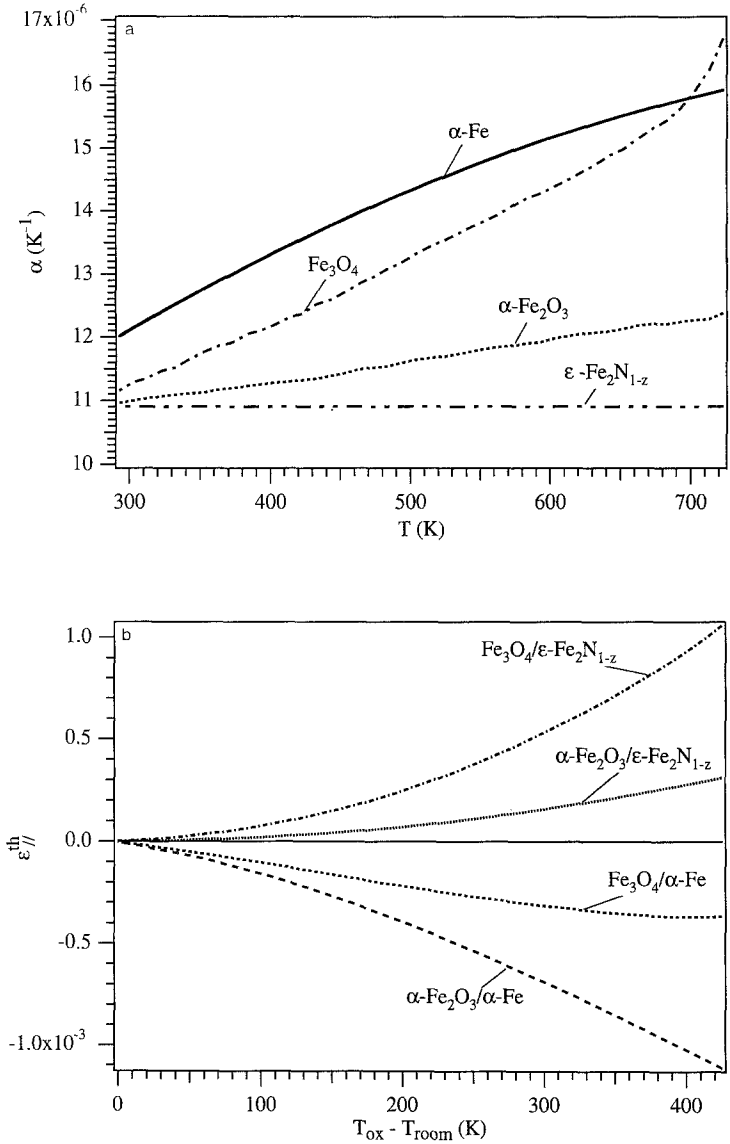

Fig. 3. The linear expansion coefficients, α, as a function of temperature, T, for ferrite,[28] ε-nitride,[32] magnetite,[29] and hematite[31] (a) (cf. text in Evaluation of Growth Strains in Oxide Phases section). Thermal residual strains parallel to the surface, $\varepsilon_{\parallel}^{th}$, as a function of the cooling range from oxidation temperature (T_{ox}) to room temperature (T_{room}), $T_{ox} - T_{room}$, for various oxide layer/substrate assemblies (b). The residual strains were calculated using Eq. (1) and the data in (a).

from HCP to FCC under the incorporation of Fe-cations (cf. Ref. 33), a rearrangement of the anions at the hematite/ferrite interface does occur during the development of magnetite and/or (ii) the interface between the ferrite substrate and the developing magnetite, ignored in the above discussion, plays a decisive role in strain generation.

The decrease of the compressive growth strain in hematite and of the tensile growth strain in magnetite on ferrite upon prolonged oxidation is ascribed to the observed occurrence of buckling over large surface areas of the sample and to the possible occurrence of creep in the oxide layer and/or the substrate.

Buckling of Oxide Layers on α-Fe

A recent HREM investigation of iron-oxide layers[37] formed during oxidation of atomically clean polycrystalline, pure iron at 573 K in pure O_2 for 16 min showed the occurrence of cracks within the Fe_3O_4 sublayer very close to and running parallel to the oxide layer/substrate interface. Moreover, a specific orientation relationship was found between the magnetite grains constituting the magnetite sublayer and the underlying ferrite-substrate grain(s). Oxide layers that did not contain an Fe_3O_4 sublayer adjacent to the substrate, but a mixture of small crystallites of hematite and magnetite, did not show cracks and no specific orientation relationship was observed between these hematite and magnetite grains and the underlying ferrite grains.[37] In view of these observations, the conjunction of the occurrence of buckling and the appearance of magnetite in the oxide layer, as observed in the present research (including Ref. 8), can be discussed speculatively as follows.

Buckling appears to be associated with the formation of a crack in the magnetite sublayer parallel to and close to the oxide layer/ferrite interface, and does not occur by detachment of the entire oxide layer from the substrate. In order to allow such a crack to easily extend laterally (implying decohesion), magnetite grains of large lateral size and of similar crystallographic orientation with respect to the underlying substrate are favorable. Recognizing the presence of many magnetite grains on a single ferrite-substrate grain, the specific orientation relationship between magnetite grains and a ferrite grain could explain why blisters terminate at the boundaries of the ferrite-substrate grains (cf. Fig. 2a in this article and Fig. 3a/b in Ref. 8). In an early stage of oxidation mainly finely grained hematite develops on ferrite. The absence of a specific orientation relationship between such hematite grains and the underlying ferrite grain and the multitude of grain boundaries in the oxide layer could obstruct blister formation at this stage.

The driving force for blister formation by buckling, as observed for blisters at room temperature (cf. Blister Formation by Buckling of the Oxide Layer section and Fig. 2), is the relaxation of growth and/or thermal strains in the oxide layer. An estimation of the strain relief associated with blister formation can be obtained from the surface area of the blister, A_b, and the surface area of the projection of the blister on the substrate surface, A_p. Taking the blister as strain free, the linear strain parallel to the surface, δ, that would occur if the layer were attached to the ferrite surface follows from $\delta = ((A_p/A_b)^{1/2} - 1)$. For the blister shown in Fig. 2, which developed upon oxidizing α-Fe at 573 K and additional cooling to room temperature, it is obtained $\delta = -0.17 \pm 0.02\%$ if the blister is assumed to be conical and $\delta = -0.35 \pm 0.05\%$ if the blister is conceived as a spherical cap. These values are of the same sign and order of magnitude as the experimental values for strain in hematite, as determined at room temperature upon oxidizing α-Fe at 673 K for 49 min (Table Ib), leading to similar buckling as at 573 K.[8] The thermal strain in the oxide layer due to the difference in thermal shrinkage between the oxide layer and the α-Fe substrate on cooling from 573 K to room temperature (which applies to the specimen shown in Fig. 2) is -0.029% for magnetite and -0.061% for hematite (cf. Fig. 3b). In absolute sense these values are 3–12 times as small as the values calculated above. Hence, buckling originates predominantly from the relaxation of growth strains in the oxide layer.

Consider the dual-phase hematite/magnetite oxide layer at the oxidation temperature to be constituted of mainly a hematite sublayer at the surface side, containing compressive growth strains, and a magnetite sublayer at the substrate side, containing tensile growth strains. If such a layer assumes its unconstrained shape, it will bulge out such that the hematite layer is on the outside and thereby has relaxed (part of) its compressive strain and the magnetite layer is on the inside and thereby has relaxed (part of) its tensile strain. This behavior agrees with the shape of the blisters observed for the present oxide layers (Fig. 2). Obviously, upon cooling the development of a compressive thermal strain in α- Fe_2O_3 that is larger than that in Fe_3O_4 (see Fig. 3b) enhances the tendency to such buckling.

The critical compressive stress for initial buckling of the oxide layer, σ_b^{crit}, was given as:[17]

$$\sigma_b^{\text{crit}} = \frac{1.22E}{(1-\nu^2)} \left(\frac{d}{R}\right)^2 \tag{5}$$

where E and ν are Young's modulus and Poisson's constant, respectively, d is the thickness of the buckling (part of the) layer and $2R$ is the critical (minimal) diameter of the circular area of decohesion associated with σ_b^{crit}.

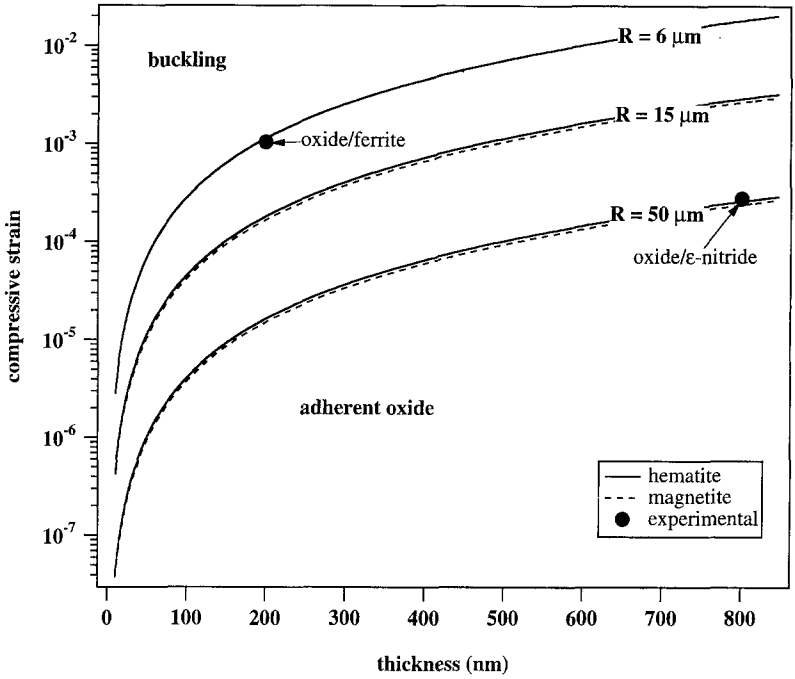

Fig. 4. The critical compressive strain for buckling parallel to the plane of the oxide layer for hematite and magnetite layers as a function of the thickness of the oxide layer. The curves shown were calculated using Eq. (5a) for various values of the critical circular area of decohesion characterized by the diameter 2R. Experimental data shown pertain to the oxide layers obtained after oxidation for 49 min at 673 K, adopting the total thickness of the oxide layer (Fig. 2 in Ref. 8) and the compressive strain as determined for hematite on α-Fe and "porous" ε-nitride (Table Ic).

Using Eq. (3) this critical compressive stress is transformed into the critical compressive strain for buckling, $\varepsilon_b^{\text{crit}}$

$$\varepsilon_b^{\text{crit}} = \frac{1.22}{(1+\nu)}\left(\frac{d}{R}\right)^2 \tag{5a}$$

The critical compressive strain for buckling of a magnetite layer ($\nu = 0.29$) and for buckling of a hematite layer ($\nu = 0.19$) are given as a function of layer thickness d for various values of R in Fig. 4.

The experimental thicknesses of the oxide layers on ferrite and on ε-nitride after 49 min of oxidation at 673 K are about 0.2 μm and about 0.8 μm, respectively (Fig. 2 in Ref. 8); the associated compressive growth strains in hematite follow from Table Ic (the tensile growth strain in magnetite is ignored here; as discussed above, it promotes buckling). These experimental data are included in Fig. 4. It is concluded from the experimental

data and the calculated curves in Fig. 4 that buckling of the oxide layer on ferrite requires a considerably smaller critical diameter of decohesion than buckling of the oxide layer on ε-nitride. Grain boundaries in the substrate can act as pinning locations for blister growth (see discussion at the beginning of this section). The critical diameter of decohesion of the oxide layer on ferrite is considerably smaller than the average grain size of the ferrite grains (cf. Figs. 2 and 4 in the present paper and Fig. 3 in Ref. 8). Consequently, buckling of the oxide layer on ferrite can occur. On the other hand, the average grain size of the ε-nitride grains is considerably smaller than the critical diameter (cf. Fig. 6 in Ref. 8). Consequently, buckling of the oxide layer on ε-nitride cannot occur. In conclusion, the experimental observations regarding buckling of oxide layers on iron and on ε-nitride can be interpreted consistently on the basis of Eq. (5a).

Growth Strains in Oxide Layers on ε-Fe_2N_{1-z}

Interpretation of the strains in the oxide layers on ε-Fe_2N_{1-z} layers is even more complicated than for the oxide layers on ferrite substrates. The reason for this complexity is the morphological and compositional changes occurring in the nitride layer during oxidation (see Ref. 8), which lead to changes in the residual stresses in the entire layer/substrate assembly. A discussion of the evolution of residual stresses in ε-nitride layers during oxidation was given in Ref. 7. The relevant results from that discussion will be applied here to interpret the strains in the oxide layers.

For a massive ε-nitride layer, in the as-nitrided condition a compressive strain occurs at the surface. The development of porosity in the nitride layer during nitriding or the development of interfacial porosity in the nitride layer close to the nitride/oxide interface during oxidation (see Ref. 8) allows accommodation of internal strains by shape changes of the material enveloping the pores. Virtually no strains develop at the surface of the ε-nitride layer for the case that a porous ε-nitride layer can be conceived as constituted of rangy free-standing columns.[7]

The increase of the nitrogen content in the nitride layer close to the developing oxide during oxidation (cf. Fig. 11 in Ref. 8) is expected to give rise to a build-up of compressive strain parallel to the nitride/oxide interface in ε-nitride at that location. This can also hold for a porous ε-nitride layer, because on oxidation of a porous ε layer iron oxide develops in the pores that are in open contact with the oxidizing atmosphere. Such filled pores can no longer accommodate imposed misfit by shape changes.[34] As a result a porous ε-nitride layer that was initially (after nitriding) strain-free at the surface can exhibit a compressive strain in the interfacial region during oxidation, due to the accumulation of nitrogen. As a consequence of the

increase of the nitrogen content in the ε-nitride layer, the oxide layer growing on ε-nitride is expected to experience a gradually increasing tensile strain contribution in addition to strain contributions from other origins. This trend of an increasing tensile strain contribution to the total growth strain in the oxide layer is consistent with the observations for the "porous" ε-nitride layer: on continued oxidation the compressive growth strain in hematite changes to tensile strain and the tensile growth strain in magnetite increases (Table Ic). Regarding the observations for the "dense" ε-nitride layer, the results obtained for the strain in hematite show the same trend. The strain in magnetite appears to show opposite behavior (Table Ic), but the as-measured absolute value of the strain/stress in the magnetite on "dense" ε-nitride (cf. Experimental Procedures section and Table Ib) is of the order of the experimental error.

The precipitation processes taking place during oxidation in the ε-nitride and the γ'-nitride layers (see Ref. 8) can contribute to stress relaxation as a consequence of misfit accommodation by atomic rearrangements at moving precipitate/matrix interfaces.[7,34]

No Buckling of Oxide Layers on ε-Fe_2N_{1-z}

The absence of buckling in the oxide layer on ε-nitride is an important result in view of the possible technological, protective application of these oxides on nitride layers. The following reasons for the absence of buckling can be proposed:

- the growth strains for magnetite (tensile) and hematite (compressive) on an ε-nitride substrate are, in absolute sense, smaller than for these oxides on a ferrite substrate. Hence, the driving force for buckling is smaller for the oxide layer on ε-nitride than for the oxide layer on ferrite (cf. Buckling of Oxide Layers on α-Fe section).
- the lateral size of the columns constituting the ε-nitride layers is much smaller than the critical diameter for decohesion of the oxide layer (cf. Fig. 4 and Buckling of Oxide Layers on α-Fe section in the present work, Fig. 6 in Ref. 8). Then, considering ε-grain boundaries as pinning locations for blister growth, buckling does not occur.
- the cooling induced thermal misfit between oxide and ε-nitride is opposite to that between oxide and ferrite (cf. Fig. 3b). Hence, with respect to ε-nitride, the oxide layer experiences a (relative) tensile strain built-up along the oxide/nitride interface during cooling after oxidation, whereas a compressive strain parallel to the interface is required for crack propagation of a pre-existing crack (cf. Eq. (5)).

CONCLUSIONS

The growth strains developing in magnetite and hematite grown on ferrite substrates upon oxidation at 673 K are tensile and compressive, respectively. The driving force for buckling of the magnetite/hematite oxide layers on α-Fe is associated with the relaxation of growth strains in the hematite and magnetite sublayers. Buckling is promoted by the opposite signs of the growth strains in the magnetite (bottom) and hematite (top) sublayers. During cooling the difference in thermal contraction between the hematite and magnetite sublayers enhances the tendency for buckling. The critical diameter of decohesion (buckling) is considerably smaller than the average grain size in the ferrite substrate (grain boundaries are pinning locations for blisters).

The growth strains developing in magnetite and hematite grown on ε-Fe_2N_{1-z} layers (on ferrite substrates) on oxidation at 673 K are smaller (in absolute sense) than those in these oxides grown directly on the ferrite substrate. In addition to the mechanisms responsible for strain build-up in the oxide layer on a ferrite substrate, for an oxide layer on a nitrided ferrite substrate the increase of the nitrogen content in the ε-nitride layer leads, during oxidation, to a tensile growth strain contribution for the oxide layer, which increases with oxidation time. Buckling of oxide layers on ε-Fe_2N_{1-z} was not observed, which may be attributed to the relatively small strain values in this oxide layer and an associated large critical diameter of decohesion, that surpasses the average grain size of the ε-nitride substrate. The absence of buckling of the iron-oxide layer is a prerequisite for the improved corrosion resistance of nitrided and subsequently oxidized ferritic workpieces.

ACKNOWLEDGMENTS

The authors are grateful to A. W. J. Gommers and B. Sprong for provision and operation of nitriding and oxidation furnaces. P. F. Colijn assisted with light-optical microscopy. We thank Dr. Th. H. de Keijser and Ing. N. M. van der Pers for the provision of X-ray diffraction facilities and assistance with the calibration of the D-5000 goniometer. These investigations have been supported financially by the Foundation for Fundamental Research of Matter (FOM), the Netherlands Technology Foundation (STW) and IOP-Metalen.

REFERENCES

1. K. Sachs and D. B. Clayton, *Heat Treat. Met.* **6**, 29 (1979).
2. B. De Benedetti and E. Angelini in *Advances in Surface Treatments* **5**, (1987), ed. Niku-Lari, Pergamon Press, Oxford, p. 3.

3. *Metals Handbook*, Ninth Edition, Vol. 4, American Society for Metals, Metals Park, Ohio, 1978, 191–221.
4. G. Wahl, *Fachber. Hüttenpraxis Metallweiterverarb.* **19**, 1076 (1981).
5. C. Dawes and D. F. Tranter, *Heat Treat. Met.* **12**, 70 (1985).
6. E. J. Mittemeijer and P. F. Colijn, *Härterei-Tech. Mitt.* **40**, 77 (1985).
7. M. A. J. Somers, B. J. Kooi, W. G. Sloof, and E. J. Mittemeijer, *Mat. Sci. Forum* **154**, 87 (1994).
8. R. H. Jutte, B. J. Kooi, M. A. J. Somers, and E. J. Mittemeijer, *Oxid. Met.* **48**, 87 (1997).
9. S. Taniguchi and D. L. Carpenter, *Trans ISIJ* **18**, 523 (1978).
10. S. Taniguchi and D. L. Carpenter, *Trans ISIJ* **18**, 530 (1978).
11. T. E. Mitchell, D. A. Voss, and E. P. Butler, *J. Mater. Sci.* **17**, 1825 (1982).
12. P. B. Abel, A. H. Heuer, and R. W. Hoffman, *J. Vac. Sci. Tech. A* **1**, 260 (1983).
13. P. B. Abel and R. W. Hoffman, *J. Vac. Sci. Tech. A* **4**, 2938 (1986).
14. S. Taniguchi, T. Shibata, and M. Murakoshi, *Corr. Eng.* **36**, 295 (1987).
15. J. Stringer, *Corros. Sci.* **10**, 513 (1970).
16. S. Taniguchi, *Trans. ISIJ* **25**, 3 (1985).
17. H. E. Evans, *Int. Mater. Rev.* **40**, 1 (1995).
18. N. B. Pilling and R. E. Bedworth, *J. Inst. Met.* **29**, 529 (1923).
19. B. Pierraggi and R. A. Rapp, *Acta Metall.* **36**, 2844 (1988).
20. H. E. Evans, *Mat. Sci. Technol.* **4**, 1098 (1988).
21. J. Robertson and M. I. Manning, *Mat. Sci. Technol.* **6**, 81 (1990).
22. V. M. Hauk and E. Macherauch, *Adv. X-ray Anal.* **27**, 81 (1983).
23. R. Delhez, Th. H. de Keijser, and E. J. Mittemeijer, *Surf. Engng.* **3**, 331 (1987).
24. R. Delhez, E. J. Mittemeijer, Th. H. de Keijser, and H. C. F. Rozendaal, *J. Phys. E.* **10**, 784 (1977).
25. B. D. Cullity, *Elements of X-ray diffraction*, Addison-Wesley, Reading, Massachusetts, 1978.
26. J. G. M. van Berkum, G. J. M. Sprong, Th. H. de Keijser, R. Delhez, and E. J. Sonneveld, *Powder Diffraction* **10**, 129 (1995).
27. F. Bollenrath, V. M. Hauk, and E. H. Müller, *Z. Metallkd.* **58**, 76 (1967).
28. Y. S. Touloukian, R. K. Kirby, R. E. Taylor, and P. D. Desai, *Thermophysical Properties of Matter*, Vol. 12, IFI/Plenum, New York, 1976, pp. 157–172.
29. M. I. Manning and E. Metcalfe, *CEGB-report RD/L/N/15/75* (April 1975).
30. W. Christl, A. Rahmel, and M. Schütze, *Oxid. Met.* **31**, 1 (1989).
31. J. Armitt, R. Holmes, M. I. Manning, D. B. Meadowcroft, and E. Metcalfe, *EPRI FP–686*, TPS, 76–655 (1978).
32. D. Rechenbach: Diplomarbeit Universität Dortmund, 1993, Dortmund.
33. Y. Watanabe and K. Ishii, *Phys. Stat. Sol.* **150**, 673 (1995).
34. M. A. J. Somers and E. J. Mittemeijer, *Metall. Trans.* **21A**, 901 (1990).
35. H. Dölle, *J. Appl. Cryst.* **12**, 489 (1979).
36. W. Pepperhoff and H.-H. Ettwig, *Interferenzschichtenmikroskopie*, Dr. Dietrich Steinkopff Verlag, Darmstadt, 1970, Chapter II.
37. P. C. J. Graat, M. P. H. Brongers, H. W. Zandbergen, M. A. J. Somers, and E. J. Mittemeijer, *Microscopy of Oxidation*, Vol. 3 (The Institute of Materials, London, 1997) pp. 493–504.